Technical Report 2010-2

Smoothed Particle Hydrodynamics in Acoustic Simulations

Philipp Hahn, Dan Negrut

11/03/2010

Abstract

This contribution reports on the potential and limits of a meshless Lagrangian technique, called Smoothed Particle Hydrodynamics (SPH), as a method for acoustic simulation. The established techniques for acoustic simulation, such as the Boundary Element Method (BEM), Finite Differences Method (FD), and Finite Element Method (FEM), draw on mesh-based numerical solution techniques. In spite of steady improvements made during the last two decades, these methods continue to have difficulties handling inhomogeneous media, capturing aero-acoustic effects or solving applications with moving boundaries. The investigation of an SPH meshless approach for modeling sound propagation is carried out in order to assess its potential in relation to these difficulties. The fluid dynamics SPH formulation used in the simulations, handles compressible and viscous fluids and is versatile while straight forward to implement in a parallel and highly scalable fashion. Several sequential and parallel computational experiments with 1-D, 2-D and 3-D models are carried out for the verification of the methodology. The contribution concludes with an analysis of the solution sensitivity with respect to SPH formulation parameters and a discussion of the challenges associated with enforcing boundary conditions.

Fig. 1. Illustration of the kernel, W, and its support domain, Ω, which is bordered by S. The field function at every point (not necessarily at a particle) can be approximated by summing up the weighted function values at the positions of the particles in the support domain. For 2-D problems the support domain is a circle and for 3-D problems it is a sphere with radius κh, where κ is a constant associated to the kernel and h is the smoothing length.

The derivatives of a field function can be constructed from its values at the particles by using a kernel that is differentiable. There is no need to use finite differences or a grid. The approximation for the spatial derivative, $\nabla f(x)$, is obtained by simply substituting $f(x)$ with $\nabla f(x)$ in Eq. (1):

$$\langle \nabla f(x) \rangle = \int_{\Omega} [\nabla f(x')] W(x - x', h) dx'. \tag{7}$$

Using the product rule of differentiation, the divergence theorem and the compact condition it can be shown that Eq. (7) can be reduced to the following expression for spatial derivatives of field functions in the domain [21]:

$$\langle \nabla f(x) \rangle = - \int_{\Omega} f(x') \cdot \nabla W(x - x', h) dx'. \tag{8}$$

The particle approximation for the spatial derivative can then be written as follows:

$$\langle \nabla f(x) \rangle = - \sum_{j=1}^{N} \frac{m_j}{\rho_j} f(x_j) \nabla W(x - x_j, h). \tag{9}$$

That is, the spatial gradient of the field function can be calculated from the field function and the derivatives of the smoothing function *W*, rather than from the derivatives of the field function.

2.2 SPH formulation for acoustic simulations

Acoustic wave propagation can be described with the same equations that are used in fluid dynamics to represent the bulk flow of compressible fluid. The SPH formulation proceeds by spatially discretizing the equations of continuum mechanics in Lagrangian form:

1.) Conservation of mass: $$\frac{d\rho}{dt} = -\rho \frac{\partial v^{\beta}}{\partial x^{\beta}}, \tag{10}$$

2.) Conservation of momentum: $$\frac{dv^{\alpha}}{dt} = \frac{1}{\rho} \frac{\partial \sigma^{\alpha\beta}}{\partial x^{\beta}} + f^{\alpha}, \tag{11}$$

3.) Conservation of energy: $$\frac{du}{dt} = \frac{\sigma^{\alpha\beta}}{\rho} \frac{\partial v^{\alpha}}{\partial x^{\beta}}, \tag{12}$$

where α denotes the coordinate direction and β indicates repeated spatial indices. Furthermore, ρ stands for density, v for velocity, σ for stress, u for internal energy and f^{α} for body forces. For Newtonian fluids, the total stress tensor, $\sigma^{\alpha\beta}$, consists of the isotropic pressure, p, and the viscous stress $\sigma^{\alpha\beta}_{visc}$ ($\delta^{\alpha\beta}$ denotes a delta-function, 1 for $\alpha = \beta$ and 0 otherwise):

$$\sigma^{\alpha\beta} = -p\delta^{\alpha\beta} + \sigma^{\alpha\beta}_{visc}. \tag{13}$$

Equations (10) through (13) are not sufficient to completely pose the acoustic problem. A closure relationship given by the equation of state and relating the hydrostatic pressure to the local density and internal energy is needed. One advantage of the SPH approach is that the equation of state can be as complicated as desired. For all simulations herein the ideal gas law is used with no prior linearization. Applying a SPH spatial discretization of the above equations leads to a set of ordinary differential equations (ODEs) that are subsequently solved via numerical time integration. The general SPH formalism for fluid dynamics can be augmented with artificial viscosity and heat for shock problems [21]. Due to the small pressure and velocity gradients present in the numerical experiments of section 3, artificial viscosity is irrelevant and thus always set to zero.

The implementation draws on symmetrized versions of equation (9) because it was shown that they are numerically advantageous [22]. Details about the specific equations used in the implementation are provided in [23].

2.3 Implementation

Common to all SPH implementations is a search algorithm that at each time step finds the interaction partners of each SPH particle. This step, called nearest neighbor search, is necessary because the derivative of a field function is determined based on the field function values of neighboring particles as discussed in section 2.1. An efficient and highly parallelizable method for the nearest neighbor search, called spatial subdivision [24], is employed herein. After field function ODE's have been determined using the SPH discretization, a leap frog integration algorithm is used to simulate the time evolution of all particles [25]. The basic SPH simulation loop is illustrated in Fig. 2.

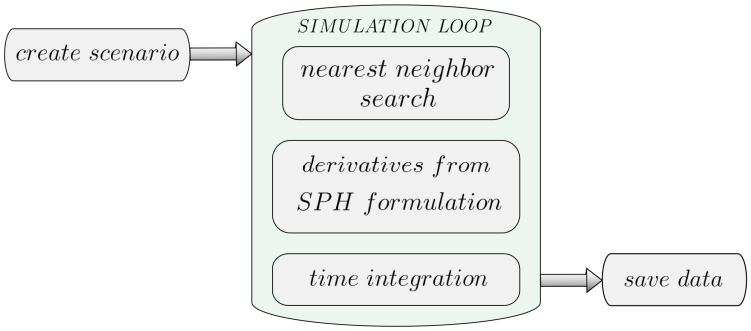

Fig. 2. Basic SPH simulation loop: after a spatial discretization that draws on a nearest neighbor search, the PDE problem becomes an ODE problem which is integrated with a leapfrog method.

The SPH formalism for acoustic problems was coded in two different implementations. The first was a serial implementation in MATLAB. The second was a parallel C++ implementation that leveraged the computational power of the Graphics Processing Unit (GPU) and drew on NVIDIA's Compute Unified Device Architecture (CUDA) application programming interface [26]. The GPU implementation was motivated by the fact that, for each time step, the MATLAB code required close to 30 seconds on a modern desktop PC to simulate a problem that used $10,000$ SPH particles whereas three-dimensional simulations with good resolution typically lead to discretizations using one million SPH particles or more. Given that all computationally intensive parts of the SPH algorithm are highly parallelizable, the GPU implementation resulted in a relative speedup of $3,500$ in comparison to the MATLAB program. The GPU used for the simulations was a NVIDIA GeForce 8800 GTX with $768\ MB$ of global memory and 128 steam processors each working at a clock rate of $600\ MHz$. The memory constraint placed a 3.5 million SPH particles limit on the size of the problems analyzed. Both implementations have been validated using classic hydrodynamics benchmark tests.

3. Numerical experiments

The reported numerical experiments are as follows. Section 3.1 will demonstrate that the SPH formalism is capable to model sound propagation accurately. The sensitivity of the SPH formulation with respect to its smoothing length is analyzed using a set of one-dimensional simulations in section 3.2. A 3-D problem is analyzed in section 3.3 to point out the challenges associated with enforcing boundary conditions in acoustic SPH simulation. A brief efficiency study; i.e., precision versus effort analysis, is summarized in section 3.4.

3.1 Two-dimensional sound propagation

The first numerical experiment demonstrates that SPH is capable of simulating sound wave propagation accurately without bulk flow effects. To this end, a simulation with $10,000$ particles is set up inside a square domain. An initial velocity profile is imposed on the particles to create a pressure field whose time evolution needs to be traced. In order to create sound waves with very small pressure amplitudes, the magnitude of the velocity is low. The amplitude needs to be small in order to stay in the linear regime. Otherwise, the nonlinear SPH model would lead to different results than the reference solution, the latter obtained by solving the linear wave equation. The velocity excitation function consists of two Gaussian distributions in x and y that are multiplied with each other to create a symmetric pulse in the middle of the domain. The Cartesian components of the initial velocity excitation are given by the following equation:

$$u_x = v_y = 0.2 \cdot e^{-\left(\frac{|x-0.09375|}{0.013}\right)^2} \cdot e^{-\left(\frac{|y-0.09375|}{0.013}\right)^2}. \tag{14}$$

In the SPH model the ratio of specific heats is $\gamma = 1.4$ and initial values for density and specific internal energy are set to $\rho = 1\ kg/m^3$ and $u = 253.3\ kJ/kg$ respectively. According to the equation of state for ideal gas [21, 23], $p = (\gamma - 1)\rho u$, this leads to standard atmospheric pressure of $p = 101,325\ Pa$. The theoretical wave speed in the ideal gas under these conditions can be calculated with respect to the internal energy:

$$c = \sqrt{\gamma \cdot \frac{p}{\rho}} = \sqrt{\gamma(\gamma - 1)u} = 377\ m/s. \tag{15}$$

Artificial viscosity is set to zero in order to ensure that viscosity effects have no influence on the results of the simulation. The particles are set up on a quadratic grid with equal particle spacing and no random component. Otherwise the high noise level resulting from particle disorder needs to be damped in a preprocessing step where the particles can find their equilibrium positions. The positions of the particles in the three outer rows that frame the domain are fixed in order to prevent the inner particles form dispersing. This is not exactly equivalent to a zero flux boundary condition because the fixed particles in the walls are compressible. Nonetheless, it is the easiest way of creating a boundary that prevents dispersion. The geometry and all simulation parameters are given in Table 1:

Table 1. Model parameters and geometry for the simulation of two-dimensional sound propagation.

Artificial viscosity parameters [27]:		
$\alpha = 0$	$\beta = 0$	$\gamma_v = 0.01$
equation of state: $p = (\gamma - 1)\rho u$		
$\gamma = 1.4$	$\rho_0 = 1\ kg/m^3$	$u_0 = 253.3\ kJ/kg$
smoothing length:		$2.5\ mm$
smoothing kernel:		cubic spline
time step size:		$5.0e^{-7}\ s$
number of particles:		$10,000$
particle mass:		$3.52e^{-6}\ kg$
particle spacing:		$1.875\ mm$
width and depth of the gas square:		$0.1875\ m$

The reference solution was obtained by a MATLAB FDTD code with MacCormack time integration [28]. Both simulations, SPH and FDTD, have the same spatial resolution and numerical integration step size. Zero flow

boundary conditions are employed for the outer rows of FD cells to model rigid walls that bound the domain. This mimics the boundaries in the SPH simulation as close as possible. Since the wave speed in the SPH simulation turned out to be slightly higher than the theoretical value in Eq. (15), the wave speed of the FDTD simulation is set to $388\ m/s$ in order to create better comparable results. The deviation from the theoretical value of $377\ m/s$ is 2.92%, an aspect discussed in section 3.2.

Fig. 3 compares the solutions obtained by FDTD and SPH through a series of plots visualizing the spatial pressure distribution at different time instances. The slightly adapted wave speed for the FDTD simulation leads to a good agreement of the plots. SPH models the pressure wave propagation accurately yet small shape and amplitude differences can be noticed. One source causing these shape differences is the grid-like structure of the particle distribution, which leads to anisotropic behavior. Further amplitude differences can be traced back to the excitation-induced bulk flow, which was taken into account in the SPH but not in the FDTD simulation. However, given the very short simulation time involved, these are second order effects since no considerable amount of bulk flow can build up. Another result of the simulation is that the fixed boundary particles employed in the SPH simulation model the rigid walls fairly well. This conclusion can be drawn because the time evolution of the pressure field stays similar to the reference solution after the waves got reflected at the walls.

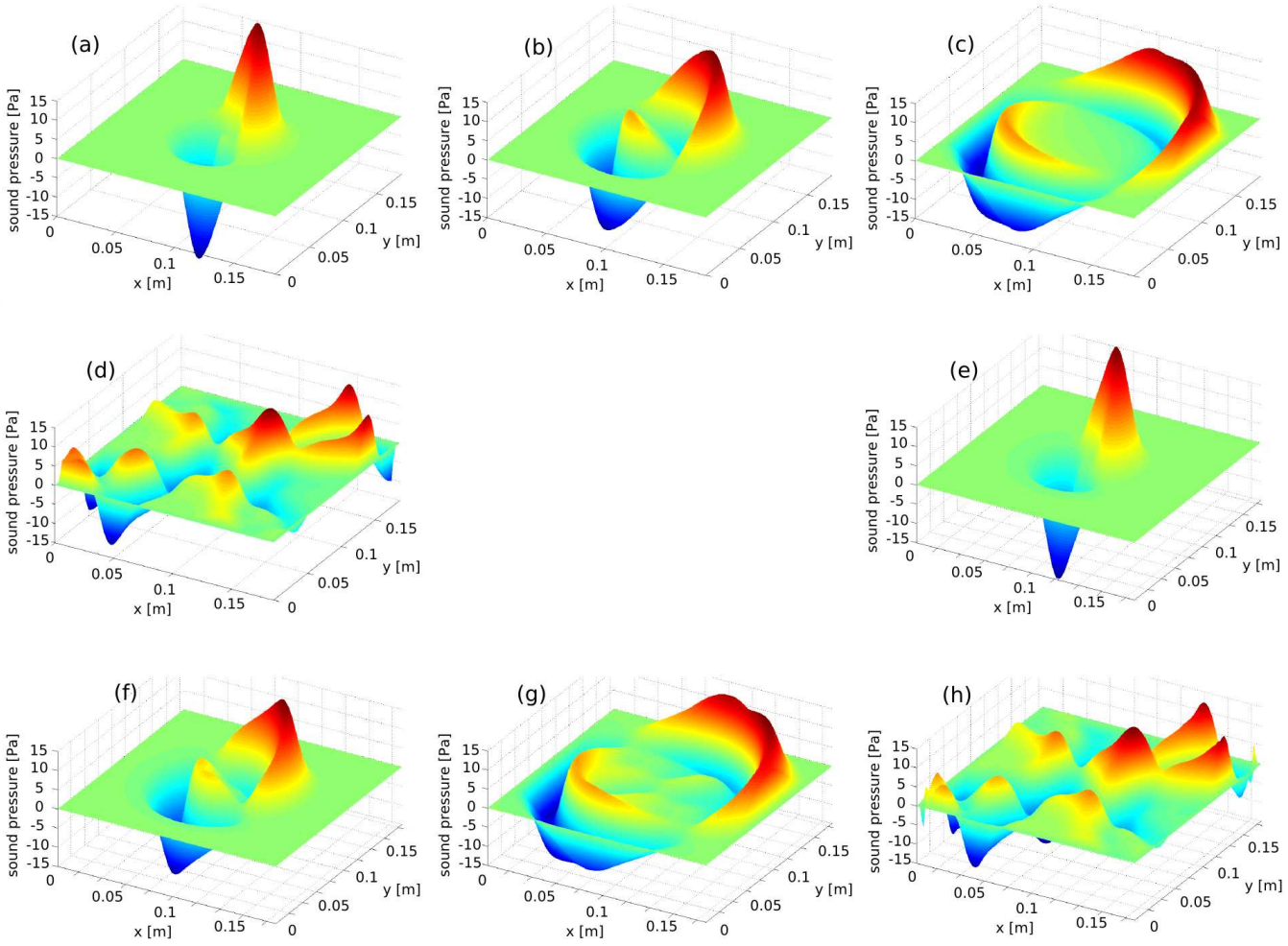

Fig. 3. Pressure distribution for the simulation of two-dimensional sound propagation. Plots (a) to (d) are calculated via FDTD and (e) to (h) via SPH. The pressure distributions are given for the following time steps: $0.053\ ms$ (a) and (e), $0.100\ ms$ (b) and (f), $0.200\ ms$ (c) and (g), $0.400\ ms$ (d) and (h).

3.2 Sensitivity of the solution with respect to SPH formulation parameters

In classical CFD, it has been shown that the shape of the smoothing kernel and the smoothing length crucially influence the accuracy of SPH simulation results [29]. A sensitivity analysis study is set up to investigate the effect of different smoothing lengths on the accuracy of SPH 1-D simulations in acoustics. To this end, 100 SPH particles are equally spaced along a line. At the beginning of the simulation all particles are at rest and under standard pressure. So called mirror boundary particles prevent the gas particles from dispersing at both ends. They are created outside the domain at each time step to mirror the properties of real particles, yet with one caveat: they have opposite velocity. In this way a symmetry axis is created that is used to define the boundary condition. A classical boundary and initial value problem for the wave equation is chosen so that an analytical solution can be determined:

$$\begin{aligned} v_{tt} = c^2 v_{xx} \quad &| \, x \geq 0; \; t \geq 0 \\ ICs: \; v(x,0) = 0 \; ; \quad &v_t(x,0) = 0 \\ BC: \; v(0,t) = f(t) &= v_0 \sigma(t). \end{aligned} \tag{16}$$

Subscripts indicate derivatives with respect to time, t, or space, x, while σ is a unit step function at the origin. The particles are excited from the left through a constant velocity excitation, v_0, that starts at time $t = 0$. The exact solution for the pressure is [30]:

$$p = p_0 + \frac{\gamma p_0 v_0}{c} \sigma(t - x/c) \, . \tag{17}$$

This is a step function with height $p_{high} - p_0 = \gamma p_0 v_0 / c$ starting at $x = 0$ and traveling towards the right end of the domain. The high pressure of the step function is defined as p_{high} and p_0 denotes mean pressure. The chosen problem has the advantage that the wave speed can be calculated indirectly using the pressure level of the step function, p_{high}, which can be determined by averaging the pressure values of the first ten SPH particles:

$$c = \frac{\gamma p_0 v_0}{p_{high} - p_0}. \tag{18}$$

All parameters used in the simulation are given in Table 2. The simulation results are reported at $t = 0.2 \; ms$, which ensures that the step function has enough time to travel into the domain. In order to gauge the sensitivity of the SPH formulation to the smoothing length, a set of 41 simulations was carried out with different smoothing lengths between one and five times the particle spacing. Fig. 4 shows the pressure profiles of the simulations at $t = 0.2 \; ms$ for three smoothing lengths: $1 \; mm$, $1.5 \; mm$, and $3.8 \; mm$.

Table 2. Model parameters and geometry for the set of one-dimensional simulations.

Artificial viscosity parameters [27]:		
$\alpha = 0$	$\beta = 0$	$\gamma_v = 0.01$
equation of state: $p = (\gamma - 1)\rho u$		
$\gamma = 1.4$	$\rho_0 = 1 \; kg/m^3$	$u_0 = 253.3 \; kJ/kg$
smoothing lengths:		$(1 : 0.1 : 5) \; mm$
smoothing kernel:		cubic spline
time step size:		$5.0e^{-7} \; s$
number of particles:		100
particle mass:		$1e^{-3} \; kg$
particle spacing:		$1 \; mm$
length of the “gas pipe”:		$0.1 \; m$
velocity excitation v_0		$2e^{-3} \; m/s$

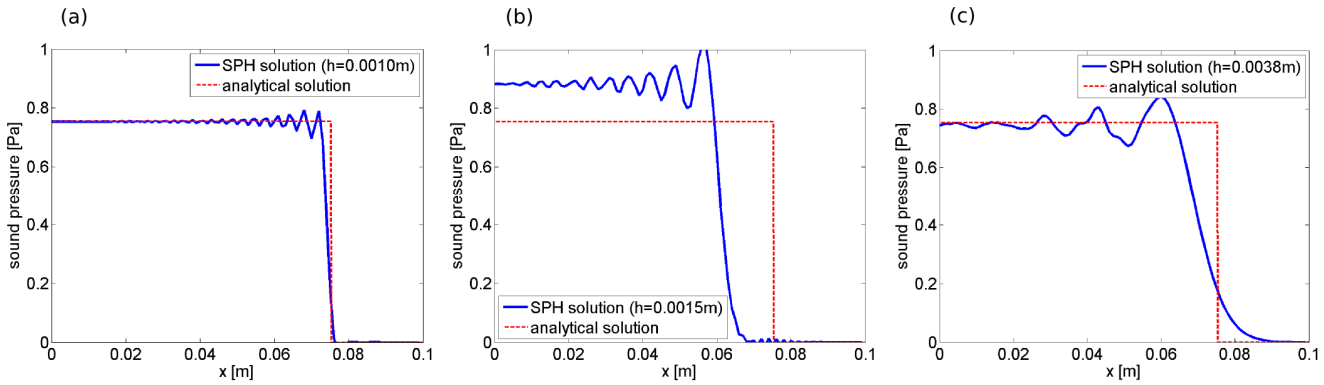

Fig. 4. Pressure profiles after $t = 0.2\ ms$ calculated with different smoothing lengths, (a): $h = 1\ mm$, (b): $h = 1.5\ mm$, (c): $h = 3.8\ mm$. The smoothing length affects both wave propagation speed and approximation quality.

The sound pressure plot (a) for smoothing length equal $1\ mm$ shows the best agreement with the analytical solution. A smoothing length of $1.5\ mm$ results in decreased wave speed and thus in an over estimated pressure level (see plot (b)). While the sound speed in plot (c) is only slightly higher than in the analytical solution, the approximation quality begins to suffer due to the long smoothing length. The relative wave velocity error in each of the 41 simulations is calculated according to Eq. (18) and plotted over the relative smoothing length as shown in Fig. 5.

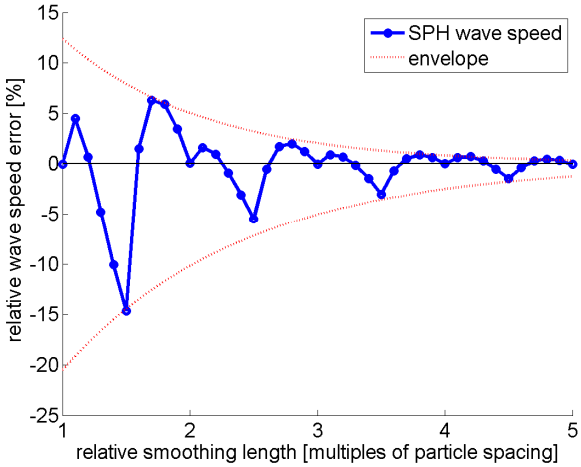

Fig. 5. Relative wave speed error for all 41 SPH simulations plotted over the relative smoothing length. Convergence of the SPH wave speed to the theoretical speed of sound can be observed with growing smoothing length.

The correlation shown in Fig. 5 aggregates results obtained in the 41 1-D SPH simulations described above, each of which having been carried out with equal particle spacing, s, and a cubic spline kernel. It indeed confirms results obtained in other application fields [29], that suggest that results are significantly more accurate if the smoothing length, h, is equal to integer multiples of s and least accurate with $h = 1.5s$. The dependency of the propagation speed on the smoothing length explains the deviations observed in section 3.1. In 2-D simulations with grid-like particle positioning, the wave speed is expected to vary slightly with the orientation relative to the grid. This explains the small shape differences in the previous 2-D experiment. According to the experiment above, in simulations with disordered particles the wave speed can show significant local changes. However, the lower and higher local wave speeds average out provided the discretization is sufficiently fine. Another trend is noticeable in Fig. 4. While the propagation speed becomes more robust for higher smoothing lengths, the approximation quality of the SPH simulation decreases. Due to the mathematic formulation underlying the SPH scheme, high smoothing lengths tend to filter out high frequency components of the signal and introduce numerical dispersion. Nonetheless

a comparison to a 1-D FDTD simulation of the same experiment and with the same discretization shows that SPH results calculated with low smoothing length can lead to superior accuracy (see Fig. 6).

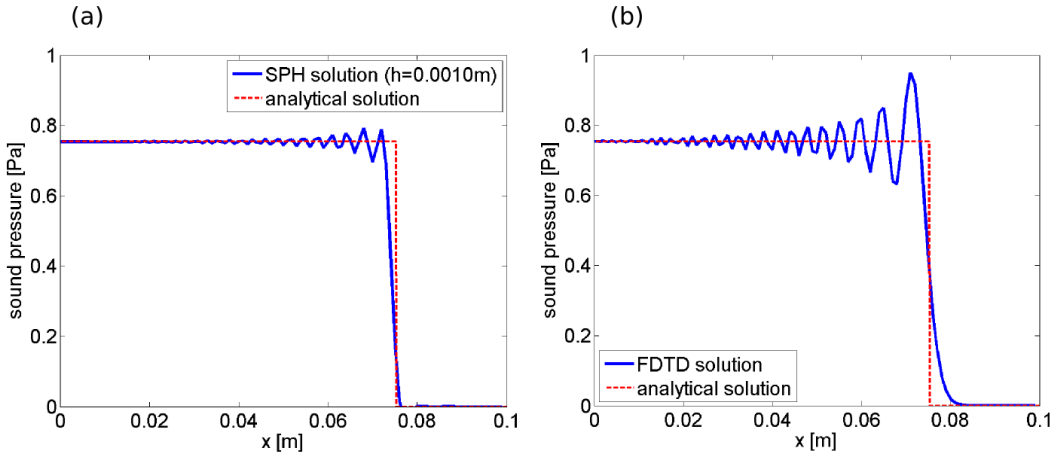

Fig. 6. Accuracy comparison between a properly tuned SPH simulation, (a), and FDTD with the same resolution, (b). For this smoothing length, which is equal to the particle spacing, SPH leads to better approximation quality than FDTD.

3.3 Sound excitation and propagation in a three dimensional tube

In order to investigate both 3-D sound propagation and sound excitation due to moving boundaries, a 3D tube experiment similar in nature to the 1-D experiment of section 3.2 was considered. Fig. 7 illustrates the geometry of this experiment and the coordinate system used.

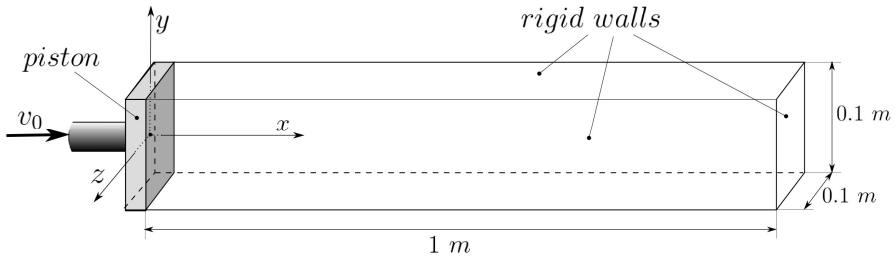

Fig. 7. Geometry and coordinate axis of the tube. It has a quadratic cross section and is filled with ideal gas.

The piston at the left end of the tube moves with a constant velocity leading to a problem similar to the one described in Eq. (16). Unlike in section 3.2, the experiment here tackles the analysis in 3-D, which significantly complicates the issue of enforcing boundary conditions. Problems arise from the so called “particle deficiency” outside the boundaries that leads in Eq. (9) to an erroneous particle approximation of the domain integrals. It is well documented that enforcing boundary conditions poses significant challenges in fluid dynamics SPH simulations [21], which is a general trait of mesh-free methods [31]. Various approaches to enforcing boundary conditions have been proposed for other SPH applications. A simple and widely used first approach is to specify repulsive forces that prevent particles from penetrating boundaries [22]. Tests with this boundary formulation indicate that they are not well suited for acoustic simulations [23]. High disturbances, due to unbalanced fluid and boundary forces in the initial configuration, need to be damped out before a reasonable simulation can start. However, the pressure distribution after the first step is very inhomogeneous. High pressure peaks remain after the kinetic energy has been dissipated from the system. Attempts to obtain a homogeneous initial pressure distribution did not lead to promising results. A second boundary formulation [32] based on boundary integrals suffers from the same problem. As seen in section 3.1 the simplest way to enforce boundaries is given by a layer of fixed particles along boundaries. However, if fluid particles move tangentially with respect to the boundary layer, the changing distances between boundary and fluid particles cause noisy simulation results. The use of mirror particles like in section 3.2 has the potential to

improve this problem because the zero-flux boundary conditions can be represented exactly. However, initial trials for this 3-D simulation revealed a problem related to particle deficiency. Specifically, void areas exist at the edges of the tube where no mirror particles are created, which indicates that particle deficiency is only partially avoided. Thus, curved surfaces and edges cannot be modeled accurately with this technique. However, for this specific simulation the voids can be filled with fixed boundary particles. The results obtained with this third approach to enforcing boundary conditions are slightly less noisy than the results obtained only with fixed boundary particles. Parameters employed in this simulation are given in Table 3 and the pressure profile on a horizontal level at $y = 0$ is provided in Fig. 8.

Table 3. Model parameters and geometry for the simulation of three-dimensional sound propagation and excitation in a tube.

Artificial viscosity parameters [27]:		
$\alpha = 0$	$\beta = 0$	$\gamma = 0.01$
equation of state [23]: $p = (\gamma - 1)(\rho - \rho_{mean})(u - u_{mean})$		
$\gamma = 1.4$	$\rho_0 = 1\ kg/m^3$	$u_0 = 253.3\ kJ/kg$
smoothing length:		$4.0\ mm$
smoothing kernel:		cubic spline
time step size:		$1.0e^{-6}\ s$
number of particles:		$270,000$
particle mass:		$3.70e^{-8}\ kg$
particle spacing:		$3.33\ mm$
geometry of the tube:		$1\ m \times 0.1\ m \times 0.1\ m$
velocity excitation v_0		$2e^{-2}\ m/s$

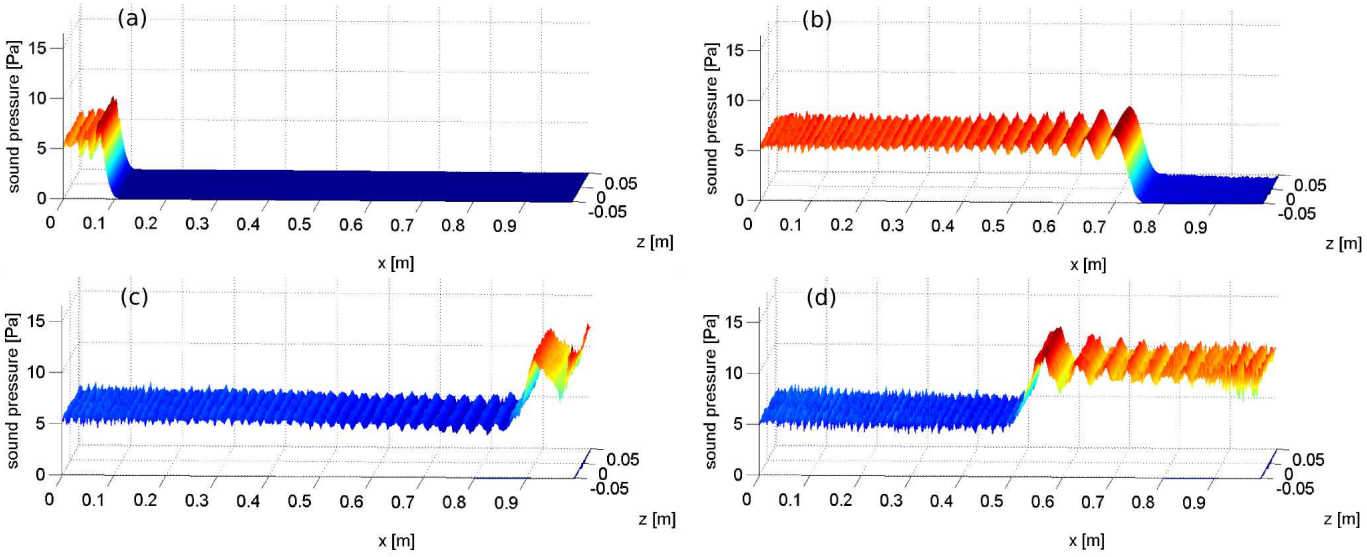

Fig. 8. Pressure distribution on a horizontal level at $y = 0$ for the simulation of 3-D sound propagation and excitation in a tube. The pressure distributions are given for the following time steps: $0.025\ ms$ (a), $0.200\ ms$ (b), $0.300\ ms$ (c), $0.400\ ms$ (d). The last two plots show the wave travelling to the left after reflection at the fixed end of the tube.

Similar to the experiment demonstrated in section 3.2, a discontinuity with a constant level is expected to propagate through the tube doubling its height when reflected by the right end of the tube. It can be shown that the pressure level is reproduced with good accuracy, meaning that sound excitation due to the piston motion is modeled correctly. However, it can also be noticed that, along with dispersion phenomena known from section 3.2, the noise level introduced by the boundary formulation is high and accumulates over time.

3.4 Accuracy and computational efficiency

A set of simple 3-D SPH acoustic simulations [23] with different resolutions was run and found to converge with second order accuracy. This agrees with theoretical as well as similar numerical results reported in literature for other application fields [20]. The time stepping for each SPH simulation needs to be adjusted according to the Courant-Friedrichs-Lewy condition [23, 33]. For this set of simulations, required computation times were recorded and illustrated in Fig. 9. It can be seen that the highly parallel GPU implementation, described in section 2.3, scales linearly with the number of SPH particles. The parallel implementation leads to high computational efficiency even for problems that require a large number of particles.

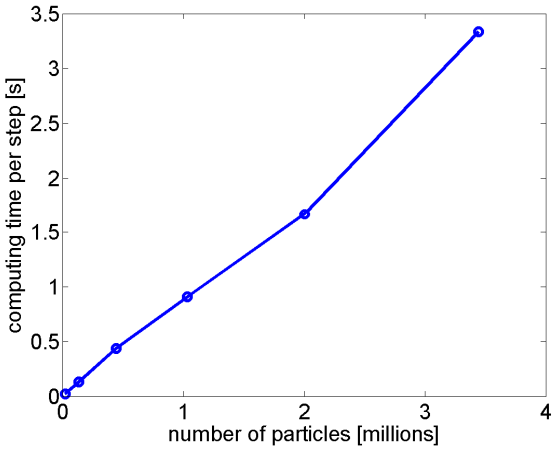

Fig. 9. Computing time for one simulation step, plotted over the number of SPH particles in the simulation ($17,576$; $132,651$; $438,976$; $1,010,301$; $2,000,376$ and $3,442,951$ particles). Calculation times are recorded for the NVIDIA GeForce 8800 GTX GPU.

4. Conclusion

Meshless Lagrangian methods represent an attractive alternative for acoustic simulations in several cases in which traditional mesh-based solution methods have significant difficulties: aero-acoustical problems, complex and changing domain topologies, domains with multiple propagation media, domains with complex temperature or density gradients, nonlinear acoustics and shock waves with fluid-structure interaction. The numerical experiments conducted in this study confirm that it is possible to simulate sound wave propagation using SPH. The results obtained are in agreement with the solution of the linear wave equation calculated using an FDTD scheme. The SPH methodology was shown to lead to results that are sensitive to the smoothing length considered in the numerical solution. Specifically, overly long smoothing lengths led to high levels of numerical dispersion and therefore numerical solution inaccuracies. Three dimensional simulations revealed that difficulties in enforcing boundary conditions represent the main drawback of acoustic SPH simulations. Using a combination of two techniques for enforcing boundary conditions, a fixed boundary particle and a mirror particle approach, sound wave excitation due to moving boundaries has been simulated in agreement with the analytical solution. Moreover, pressure wave reflection at rigid walls was reproduced accurately. However, the high level of noise caused by moving boundaries when modeled using the two techniques mentioned, constitutes a barrier that needs to be addressed before SPH can be adopted for every day acoustic simulations. Drawing on a GPU-based SPH implementation, the solution of 3-D problems was shown to scale linearly with the number of particles, and could be obtained efficiently using commodity parallel computing hardware.

In terms of open problems and future work, the most pressing issue remains that of enforcing boundary conditions in an accurate and general fashion. In this context it has been reported that a corrective SPH formulation, called CSPH, reduces disturbances near boundaries drastically [21]. Since SPH is based on conservation laws and constitutive relations that do not have to be linearized, it should be able to capture nonlinear effects but further work

needs to be done to validate the method for nonlinear wave propagation. Finally, another relevant application that remains to be investigated in conjunction with SPH is that of sound propagation through inhomogeneous media.

Acknowlagement

The authors would like to acknowledge the funding provided by the National Science Foundation under NSF Project CMMI-0700191.

References

[1] P. Bettess, O. Zienkiewicz, Diffraction and refraction of surface waves using finite and infinite elements. *International Journal for Numerical Methods in Engineering* 11 (1977) 1271-1290. doi: 10.1002/nme.1620110808

[2] L. Gaul, M. Kögl, M. Wagner, *Boundary element methods for engineers and scientists: An introductory course with advanced topics*, Springer, Berlin, 2003.

[3] A. Craggs, A finite element method for the free vibration of air in ducts and rooms with absorbing walls. *Journal of Sound and Vibration* 173 (1994) 568-576. doi: 10.1006/jsvi.1994.1553

[4] R. Ciskowski, C. Brebbia, *Boundary element methods in acoustics*, Elsevier Applied Science, London, New York, 1991.

[5] D. Botteldooren, Finite-difference time-domain simulation of low-frequency room acoustic problems. *Journal of the Acoustical Society of America* 98 (1995) 3302-3308. doi: 10.1121/1.413817

[6] D. Murphy, A. Kelloniemi, J. Mullen, S. Shelley, Acoustic modeling using the digital waveguide mesh. *IEEE Signal Processing Magazine* 24 (2007) 55-66. doi: 10.1109/MSP.2007.323264

[7] T. Funkhouser, N. Tsingos, I. Carlbom, G. Elko, M. Sondhi, J. West, G. Pingali, P. Min, A. Ngan, A beam tracing method for interactive architectural acoustics. *The Journal of the Acoustical Society of America* 115 (2004) 739-756. doi: 10.1121/1.1641020

[8] R. Hickling, D. Feldmaier, F. Chen, J. Morel, Cavity resonances in engine combustion chambers and some applications. *The Journal of the Acoustical Society of America* 73 (1983) 1170-1178. doi: 10.1121/1.389261

[9] L. Landau, E. Lifshitz, Fluid Mechanics, Vol. 6, Course of Theoretical Physics, 1987.

[10] M. Howe, *Acoustics of fluid-structure interactions*, Cambridge University Press, New York, 1998.

[11] M. Yokokawa, A. Uno, T. Ishihara, Y. Kaneda, 16.4-Tflops direct numerical simulation of turbulence by a Fourier spectral method on the Earth Simulator, Proceedings of the 2002 ACM/IEEE conference on Supercomputing, Baltimore, Maryland, 2002, pp. 1-17.

[12] M.J. Lighthill, A General Introduction to Aeroacoustics and Atmospheric Sound, Proceedings of the International Congress on Recent Developments in Air- and Structure-Borne Sound and Vibration Vol. 1 (A93-55851 24-31), Auburn University, Al., 1992, pp. 5-34.

[13] M.J. Lighthill, On sound generated aerodynamically. I. General theory. *Proceedings of the Royal Society of London. Series A, Mathematical and Physical Sciences* (1952) 564-587.

[14] F. Fahy, T. Rossing, *Foundations of engineering acoustics*, Academic Press, London, 2002.

[15] J. Monaghan, SPH compressible turbulence. *Royal Astronomical Society, Monthly Notices* 335 (2002) 843-852. doi: 10.1046/j.1365-8711.2002.05678.x

[16] D. Violeau, R. Issa, Numerical modelling of complex turbulent free-surface flows with the SPH method: An overview. *International Journal for Numerical Methods in Fluids* 53 (2007) 277-304. doi: 10.1002/fld.1292

[17] C.T. Wolfe, S.K. Semwal, Acoustic Modeling of Reverberation using Smoothed Particle Hydrodynamics, Wscg 2008, Full Papers, 2008, pp. 191-198.

[18] L. Lucy, A numerical approach to the testing of the fission hypothesis. *The Astronomical Journal* 82 (1977) 1013-1024. doi: 10.1086/112164

[19] R. Gingold, J. Monaghan, Smoothed particle hydrodynamics- Theory and application to non-spherical stars. *Royal Astronomical Society, Monthly Notices* 181 (1977) 375-389.

[20] W. Benz, Smooth particle hydrodynamics-a review, Proceedings of the NATO Advanced Research Workshop on The Numerical Modelling of Nonlinear Stellar Pulsations Problems and Prospects, Les Arcs, 1990, pp. 20-24.

[21] G.R. Liu, M.B. Liu, *Smoothed particle hydrodynamics: A meshfree particle method*, World Scientific, New Jersey, 2003.

[22] J.J. Monaghan, Smoothed Particle Hydrodynamics. *Reports on Progess in Physics* 68 (2005) 1703-1759. doi: 10.1088/0034-4885/68/8/R01

[23] P. Hahn, On the Use of Meshless Methods in Acoustic Simulations, M.S. Thesis Mechanical Engineering, University of Wisconsin-Madison, 2009. Available from: http://sbel.wisc.edu/documents/PhilippHahn_MS_thesis_final.pdf.

[24] J. Monaghan, J. Lattanzio, A refined particle method for astrophysical problems. *Astronomy and Astrophysics* 149 (1985) 135-143.

[25] A. Iserles, *A first course in the numerical analysis of differential equations*, Cambridge University Press, New York, 1996.

[26] NVIDIA Corporation, NVIDIA CUDA: Compute Unified Device Architecture, Programming Guide Version 2.3, NVIDIA Corporation, Santa Clara, 2009.

[27] J. Monaghan, R. Gingold, Shock simulation by the particle method SPH. *Journal of Computational Physics* 52 (1983) 374-389. doi: 10.1016/0021-9991(83)90036-0

[28] J. Hoffman, *Numerical methods for engineers and scientists*, McGraw-Hill, New York, 2001.

[29] J. Monaghan, Smoothed particle hydrodynamics. *Annual Review of Astronomy and Astrophysics* 30 (1992) 543-574.

[30] T. Myint-U, L. Debnath, *Partial differential equations for scientists and engineers*, North Holland (Elsevier Science Publishing Co), New York, 1987.

[31] T. Belytschko, Y. Krongauz, D. Organ, M. Fleming, P. Krysl, Meshless methods: an overview and recent developments. *Computer Methods in Applied Mechanics and Engineering* 139 (1996) 3-47. doi: 10.1016/S0045-7825(96)01078-X
[32] M. Biggs, A. Roy, C. Hughes, First principles treatment of boundary conditions in SPH, University of Edinburgh, 2007.
[33] R. Courant, K. Friedrichs, H. Lewy, On the partial difference equations of mathematical physics. *IBM Journal of Research and Development* 11 (1967) 215-234.